Nanoscale Res Lett (2010) 5:1721–1726
DOI 10.1007/s11671-010-9701-3

NANO EXPRESS

Periodically Aligned Si Nanopillar Arrays as Efficient Antireflection Layers for Solar Cell Applications

Xiaocheng Li · Junshuai Li · Ting Chen · Beng Kang Tay · Jianxiong Wang · Hongyu Yu

Received: 24 May 2010 / Accepted: 13 July 2010 / Published online: 28 July 2010

Abstract Periodically aligned Si nanopillar (PASiNP) arrays were fabricated on Si substrate via a silver-catalyzed chemical etching process using the diameter-reduced polystyrene spheres as mask. The typical sub-wavelength structure of PASiNP arrays had excellent antireflection property with a low reflection loss of 2.84% for incident light within the wavelength range of 200–1,000 nm. The solar cell incorporated with the PASiNP arrays exhibited a power conversion efficiency (PCE) of ~9.24% with a short circuit current density (J_{SC}) of ~29.5 mA/cm^2 without using any extra surface passivation technique. The high PCE of PASiNP array-based solar cell was attributed to the excellent antireflection property of the special periodical Si nanostructure.

Keywords Si nanopillar arrays · Antireflection · Periodicity · Solar cell · Chemical etching

Introduction

Climate change, energy crisis and increasing monetary cost arisen from the nonrenewable fossil fuels have attracted extensive broad public attentions. The demands for developing renewable clean energy resources have been greatly increased in recent years [1, 2]. Among the various energy projects in progress, photovoltaic (PV) is an almost maintenance-free and truly renewable clean energy and is considered as the most promising candidate for future energy resources [3, 4]. Although many Si-based PV devices have been developed during the past decades, single-crystal Si wafer–based PV modules still show the highest efficiency. However, more than 30% of incident light is reflected back due to the high reflective index of Si, which greatly reduces the PCE of the photovoltaic device. For traditional Si wafer–based solar cells, the pyramidal or inverted pyramidal structures were generally constructed on Si surface to reduce the reflection loss for incident light [5, 6]. Extra single-layer antireflection coating (SLARC) or double-layer antireflection coating (DLACR), such as Si_3N_4, MgF_2 and Si_3N_4/MgF_2 DLACR, was also needed to further suppress the reflection loss [7]. Unfortunately, these complex processes often make the rigorous requirements for experimental condition and limit the practical application of Si-based solar cells.

Recent studies on the optical and electrical characteristics of Si nanostructures, including Si nonowires (SiNWs) [8–12], Si nanopillars (SiNPs) [13] and Si nanocones/Si nanotips (SiNCs/SiNTs) [14–16], demonstrate their promising applications in solar cell. These typical structures involve the utilization of SiNWs/NPs/NTs that are long enough to absorb most of incident light. Meanwhile, their small diameters provide a short collection length for excited carriers in a direction normal to the light absorption, even for relatively impure absorber materials [13]. Theoretical studies have indicated that PASiNP or PASiNW arrays are beneficial for light reflection suppression than the disordered ones [12, 16, 17]. Inspired by these promising applications, many methods have been developed to synthesize the SiNW and PASiNP arrays. In these methods, electroless chemical etching is a simple method to fabricate large-area SiNWs/NPs arrays without using any special equipment [18–22]. However, this wet etching process is hard to precisely control the position and

X. Li (✉) · J. Li · T. Chen · B. K. Tay · J. Wang · H. Yu
School of Electrical and Electronic Engineering, Nanyang Technological University, 50 Nanyang Avenue, Singapore 639798, Singapore
e-mail: xiaocheng@ntu.edu.sg

diameter of SiNWs, thus producing the disordered SiNWs bundles and limiting their applications in solar cells. It is worth mentioning that the reports on photovoltaic applications utilized highly ordered NWs/NPs arrays are still rare [22].

In this study, a simple floating–transferring technique was adopted to create large-scale PS sphere monolayer without using any special equipment [23]. Combined with a dry catalyst deposition as well as the previous wet chemical etching process, large-area PASiNP arrays were fabricated on Si surface using the diameter-reduced PS spheres as mask. Due to their typical sub-wavelength structure, the PASiNP arrays show a low reflectance loss of 2.84% within the wavelength range of 200–1,000 nm. Based on their excellent antireflection property, the solar cell incorporated with PASiNP shows a high PCE of ~9.24% without any further modification for light trapping scheme and structural optimization, indicating their great potential in photovoltaic application.

Experimental Details

P-type Si (100) wafers with thickness of ~750 μm and resistivity of 1–30 Ω cm were used as substrates. The Si wafers were cut into 2 × 2 cm^2 squares and precleaned with Piranha solution (H_2SO_4/H_2O_2 = 3:1, v:v) at 90°C and RCA solution ($NH_3/H_2O_2/H_2O$ = 1:1:5, v:v) at 75°C for 1 h in turn, to obtain a hydrophilic surface. The Si substrates were then rinsed in deionized water for several times.

For their application in solar cells, the PASiNP arrays were fabricated on planar Si p–n junction wafer in our experiment. The fabrication process of PASiNP arrays is depicted in Fig. 1. It mainly consists of the following steps:

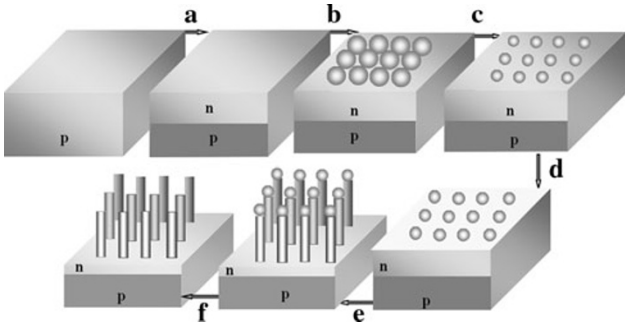

Fig. 1 Schematic illustration of fabrication process of PASiNP arrays: **a** creation of planar silicon p–n junction wafer via a standard phosphorus ($POCl_3$) doping process at 930°C; **b** self-assembly of PS spheres on silicon wafer; **c** reduction in the diameter of PS spheres by a RIE process; **d** deposition of silver film; **e** fabrication of PASiNP arrays in the mixture solution of HF and H_2O_2; and **f** removal of residual PS spheres and silver particles

(a) creation of planar silicon p–n junction wafer via a standard phosphorus ($POCl_3$) doping process at 930°C for 30 min; (b) self-assembly of PS sphere (~170 nm in diameter) monolayer on Si wafers using a floating–transferring technique [23]; (c) reduction in the diameters of PS sphere to ~115 nm by a reactive ion etching (RIE) system with RF power of 30 W and argon flow rate of 20 sccm for 115 s; (d) deposition of silver film with thickness of ~ 25 nm by a sputtering system; (e) fabrication of PASiNP arrays by immersing the Si wafers into the mixture solution of 4.6 M HF and 0.44 M H_2O_2 for 50 s; and (f) removal of residual PS spheres and residual Ag particles by toluene, APM solution ($NH_4OH/H_2O_2/H_2O$ = 2:1:5, v:v) and HPM solution ($HCl/H_2O_2/H_2O$ = 2:1:8), in turn.

The fabrication of PASiNP-based solar cell is similar to the traditional Si solar cell technology. After removal of residual PS spheres and silver particles on the surface of PASiNP arrays, a thin layer of aluminum film with thickness of ~250 nm was deposited on the backside of Si substrate and annealed at 600°C to form an ohmic contact with Si wafers. Then, a thin layer of Ti/Pd/Ag (60/60/100 nm) multifilm was deposited on the surface of PASiNP arrays via a mask evaporation process. Finally, the samples were annealed in N_2 atmosphere at 200°C for 6 h and cut into 1 × 1 cm^2 for PCE measurement.

The morphologies of the samples were characterized by LEO 1550 field emission scanning electron microscopy (FESEM) and JEOL 2010 high-resolution transmission electron microscopy (HRTEM). The TEM samples were prepared by dispersing the as-fabricated SiNWs in ethanol under ultrasonication and transferred to a carbon-coated copper grid. Optical reflectance spectra were recorded by a PerkinElmer LAMBDA 950 UV/Vis/NIR spectrophotometer. The PEC measurement of PASiNP array–based solar cell was performed using a solar simulator under Air Mass (AM) 1.5 G illumination with intensity of 100 mW/cm^2.

Results and Discussion

Figure 2a and b shows the top-view SEM images of the SiNP arrays. The low-magnification SEM image in Fig. 2a clearly shows the homogenous distribution of SiNP arrays over large areas. High-magnification SEM image shown in Fig. 2b reveals that the periodicity of the SiNP arrays is about 170 nm, which is consistent with that of the size of PS sphere monolayer before RIE process. The packing density of SiNPs is calculated to be 3.46 × 10^9/cm^2. The mean diameter of SiNP and interspace between two neighboring SiNPs are about 120 and 50 nm, respectively. It is worth mentioning that the periodicity and diameter of the SiNP could be controlled by the size of diameter-reduced PS sphere and RIE etching duration, respectively.

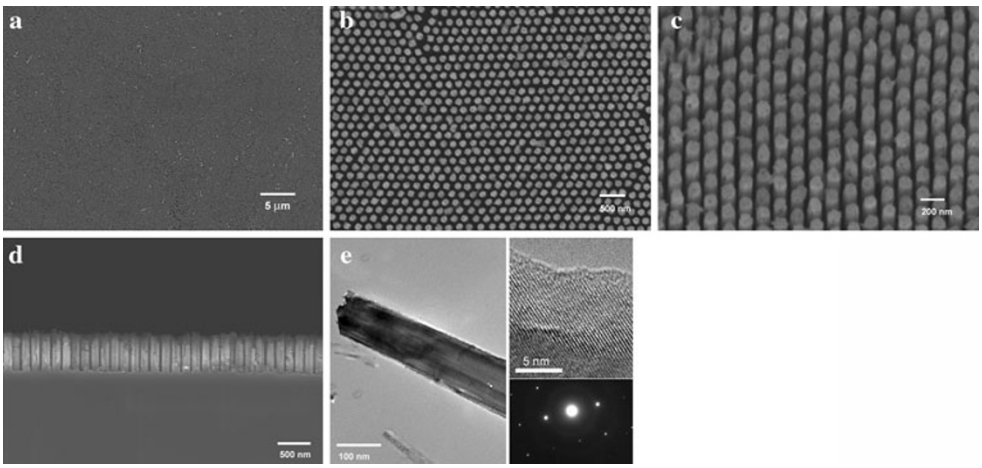

Fig. 2 Images of PASiNP arrays on Si surface: **a** Low-magnification and **b** high-magnification top-view SEM images of PASiNP arrays; **c** Tilted view and **d** cross-sectional view SEM images of the PASiNP arrays; **e** TEM image and corresponding SAED pattern of a single SiNP

Figure 2c and d shows the tilted and cross-sectional view of the SiNP, respectively. It is seen that the SiNP arrays with length of ~600 nm are vertically aligned on Si surface and no SiNP bundles or clumps can be observed on Si surface, implying an effective method to fabricate large-area PASiNP arrays in our study. Some silver particles are still found adhered on the surface of SiNP. According to previous report [20], the silver particles/films play the role of catalyst during the chemical etching process and only the silicon surfaces covered with silver particles/films are finally etched away. The cavities on the side wall of SiNPs are related to the lateral movement of silver particles during the chemical etching process caused by undulation of solution. In our case, the length of SiNPs is limited within ~600 nm, less than the phosphorous doping depth of 0.7 μm, by which the direct contact between the front grid electrode and the p-type Si substrate could be prevented during the following solar cell fabrication process. Figure 2e shows the TEM image and corresponding selected area electron diffraction (SAED) pattern of a single SiNP after chemical etching process. The diameter at the top end of the SiNP is slightly smaller than that of the bottom end, which is due to the longer etching time for the top end; see the left part of Fig. 2e. High-resolution TEM image and corresponding SAED pattern, as shown in right part of Fig. 2e, indicate that SiNPs still remain the single crystalline structure after chemical etching process. The amorphous layer with thickness of ~1 nm on the sidewall of SiNPs may be caused by the native oxidation in air, as indicated in upper right of Fig. 2e.

The reduction in optical loss is one of the important factors in enhancing the efficiency of PV device by increasing light coupling into the active region of the devices. The black color of our as-prepared samples implies their possible application in solar cell as the antireflection

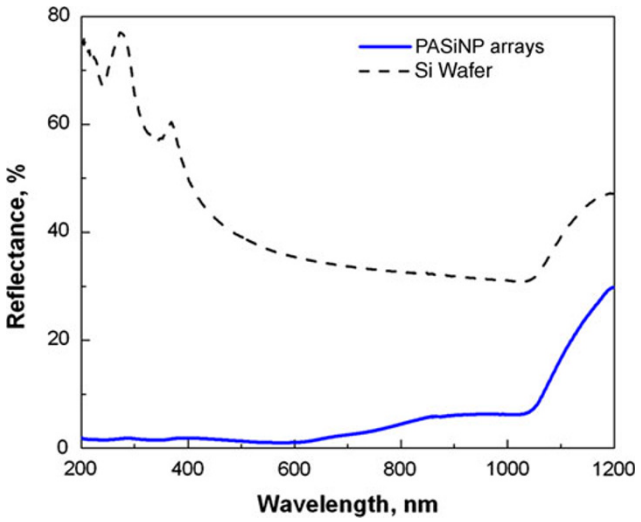

Fig. 3 Reflectance spectra recorded from pristine Si wafer (*dash line*) and PASiNP arrays covered Si wafer (*solid line*)

layer. Figure 3 shows the comparison of the measured reflectance spectrum recorded from pristine Si wafer and PASiNP arrays covered Si wafer. The pristine Si wafer exhibits the high reflection >35% within the wavelength range of 200–1,000 nm due to its high refractive index (dash line in Fig. 3). The PASiNP structure remarkably reduces the reflection of Si surface and demonstrates a low average reflection loss of ~2.84% (solid line in Fig. 3) within the same wavelength range, which is far lower than that of pristine Si wafer and previously developed Si micro-/nanostructures, as well as other ARCs [7, 8, 20, 24–27]. In previous reports, the porous Si can reduce the reflection loss to ~5.8% within the wavelength range of 400–1,000 nm and therefore can replace other surface-textured microstructures [20, 24–26]. For the other ARCs, the Si_3N_4/MgF_2 DLARC shows the low reflection loss

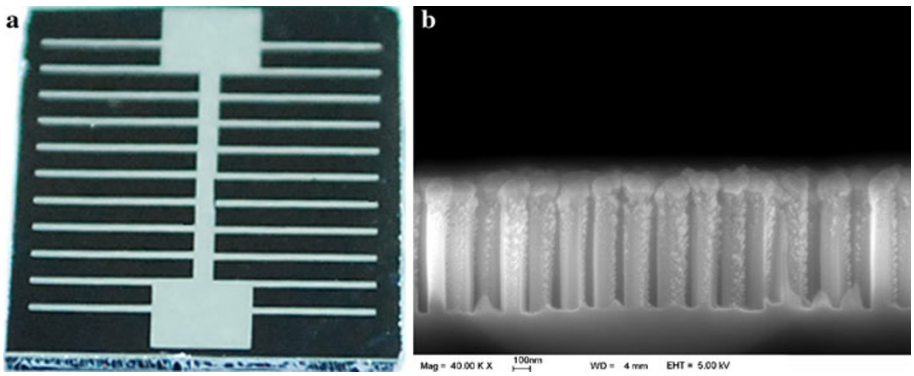

Fig. 4 **a** Optical image of SiNP-based solar cell recorded by a digital camera and **b** cross-sectional view SEM image of SiNPs arrays covered with Ti/Pd/Ag front electrode

$\sim$10% for the long wavelengths 700 nm and high reflection loss $>$ 20% for shorter wavelengths 400 nm, lower than that of individual Si_3N_4 or MgF_2 SLARC [27]. In our case, the reflection loss for PASiNP arrays is only 2.84%, which could be further decreased by increasing the length of SiNPs, within the wavelength range of 200–1,000 nm. The average reflection loss of PASiNP arrays is even as low as 1.4% for the wavelength around 200–400 nm, demonstrating the most excellent antireflection property of this special periodical nanostructure, especially in short wavelength range. The low reflection loss of PASiNPs could be explained by considering the three important features of the PASiNP arrays: (1) the huge specific surface area of SiNP arrays; (2) the surface morphology gradient of single SiNP, as shown by TEM image in Fig. 2e, which implies a graded refractive index profile between air and SiNP and thus contributes to suppress the reflection loss for incident light [16]; and (3) the two-dimensional sub-wavelength structure, which has proved to effectively suppress the reflection loss and simultaneously posses good light trapping ability [12, 15, 28]. According to previous reports, in short wavelength region, the periodicity of PASiNP arrays is comparable with the wavelength of incident light. Therefore, the scattering effect to the incident light occurs within each nanowire. As a result, the original optical path is extended, and the light absorption is enhanced. While the light absorption enhancement in long wavelength region may be related to the light trapping coupled with the strong absorption by point, line and planar defect states [28]. During the reflectance measurement, we also found that the PASiNP arrays have the lower sensitivity to the angle of incidence compared with the perfect photocrystal arrays. This may be related to the relatively coarse surface of SiNPs and the surface defects resulted from the chemical etching process. This improved antireflection and low-angle sensitivity properties of PASiNP arrays will greatly extend their applications, not only in solar cells, but also the electro-optical devices for military and photodiodes to flat panel displays [16, 29]. Besides their most excellent antireflection property, this diameter-controlled PASiNP arrays can also be used as template to fabricate radial Si p–n junction nanowire arrays, which provides the shorter collection lengths for excited carriers and has lower sensitive to impurity. This will allow for the use of low-grade material and thus decrease the cost of Si-based solar cells [9, 13].

Since the PASiNP arrays show the excellent antireflection property and have a great advantage over textured Si and other ARCs, in this study, we incorporate this typical structure into Si wafer and explore their possible application in solar cell. Figure 4a demonstrates the optical image of the fabricated solar cell recorded by a digital camera. The black area indicates the PASiNP arrays, and the white block lines stand for the Ti/Pd/Ag front grid electrode. The cross-sectional view of the white grid area of the fabricated device, as shown in Fig. 4b, indicates that the Ti/Pd/Ag multilayer electrode compactly covers on top of SiNPs and some parts of Ti/Pd/Ag film paste on the sidewall of SiNPs. This is believed to increase the contact area between the SiNPs and electrode to some extent, improving the carrier collection efficiency and thus enhanced solar cell performance. This can be indirectly reflected by the high J_{SC} of the solar cell mentioned later. Figure 5 shows the current density–voltage (J–V) characteristic curves of the solar cells with and without PASiNP arrays measured in darkness and under AM 1.5G illumination conditions, respectively. Both solar cells exhibit a clear diode behavior in darkness. Only a negligible leakage current was observed at the reverse voltage, indicating good quality of devices and good controllability of the fabrication process. When illuminated under AM 1.5G conditions, the PASiNP array–based device exhibits an open circuit voltage (V_{OC}) of $\sim$502.4 mV and the short circuit current density (J_{SC}) of $\sim$29.5 mA/cm^2 without using any extra antireflection layer and surface passivation technique, see Fig. 5a. The fill factor (FF) and power conversion efficiency (η) were calculated according to the following equations:

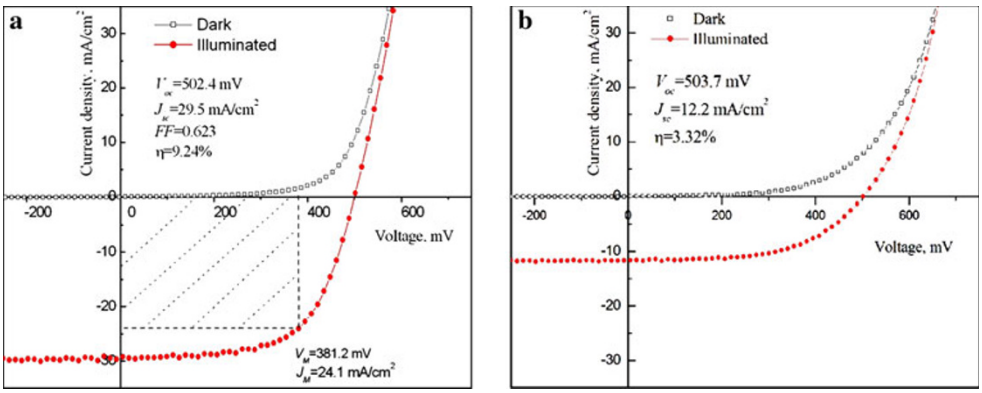

Fig. 5 *J–V* curves of the Si-based solar cells **a** with and **b** without PASiNP arrays in darkness and under AM 1.5G illumination

$$FF = V_M J_M / V_{OC} J_{SC} \quad (1)$$

$$\eta = V_{OC} J_{SC} (FF) \quad (2)$$

where V_M and J_M are the voltage and the current density at the maximum power output (indicated as the shadowed rectangle area in Fig. 5a), respectively. From the *J–V* curve of the corresponding device under illumination, *FF* and η were calculated to be ~62.3 and ~9.24%, respectively. For the solar cell without PASiNP arrays, as shown in Fig. 5b, the V_{OC} is almost the same as the device with PASiNP arrays, but the J_{SC} is only half of that obtained from PASiNP array–based solar cell, indicating the boosted PCE resulting from the suppressed light reflection due to the presence of the PASiNP arrays. The lower J_{SC} of pristine Si wafer–based solar cell in this study can be attributed to its high reflective surface since no extra surface modifications and antireflection techniques were used. Series resistance (R_s) and shunt resistance (R_{sh}), two important parameters that govern the electrical behavior of a solar cell, are also extracted from the corresponding *I–V* curves [30, 31]. The R_s for the solar cells with and without SiNPs arrays is 2.87 and 2.25 Ω, respectively, which is still slightly higher than that of standard single-crystal Si wafer–based solar cell and also the previous results [8, 30], implying that the optimization of the contact between the electrodes and SiNPs is still needed and that the improvement of the PCE could be achieved. The R_{sh} is calculated to be ~1,051 and ~2,878 Ω for the solar cells with and without SiNP arrays, respectively. This indicates that the p–n junction is still below the PASiNP arrays and that no metal particles penetrate into the depletion area during the chemical etching, even after the post-annealing process, which effectively avoid the generation of shunt paths at the bottom of device. Comparing with the high R_{sh} of pristine Si wafer–based solar cell, the relatively lower R_{sh} of the PASiNP array–based solar cell may be attributed to the numerous surface defects and dangling bonds of SiNPs originated from the chemical etching process. Although it is still not as high as that of the standard single-crystal Si wafer–based solar cell [30], we believe that the PCE of PASiNP array–based solar cell could be further improved by optimizing the electrode contact, phosphorus diffusion process and the arrangement of SiNP arrays. More importantly, this special PASiNP structure exhibits excellent antireflection property and thus granted high J_{SC} value under illumination. We expect this special PASiNP structure also has great potential applications in other fields, such as lithium ion battery and optoelectronics devices.

Conclusions

In summary, large-area PASiNP arrays were fabricated by the silver-catalyzed chemical etching process using reduced PS spheres as mask. The diameter, length and periodicity of SiNPs were precisely controlled. The PASiNP arrays show excellent antireflection property and give a low reflection loss of 2.84% within the wavelength range of 200–1,000 nm. The solar cell based on the PASiNP arrays shows a power conversion efficiency of ~9.24% with J_{SC} of ~29.5 mA/cm^2 under illumination. The large J_{SC} of the PASiNP array–based solar cell is attributed to the excellent antireflection of the PASiNP arrays for incident light. It is expected that this special PASiNP structure will have great potential in various applications in the near future, not just as the antireflection layer of solar cell.

Acknowledgment The authors thank the financial support of the MOE Tier II project of Singapore (Grant No. ARC 13/08).

References

1. M.S. Dresselhaus, I.L. Thomas, Nature **414**, 332 (2001)
2. J. Potocnik, Science **315**, 810 (2007)

3. N.S. Lewis, Science **315**, 798 (2007)
4. W. Koch, C. Hassler, H.U. Häßler, A. Müller, I.A. Schwirtlich, Diffusion Defect Data Pt. B Solid State Phenom **57–58**, 401 (1997)
5. C.-H. Sun, W.-L. Min, N.C. Linn, P. Jiang, B. Jiang, Appl. Phys. Lett. **91**, 231105 (2007)
6. A.K. Chu, J.S. Wang, Z.Y. Tsai, C.K. Lee, Sol. Energy Mater. Sol. Cells **93**, 1276 (2009)
7. A. Atzek, J.J. Capart, R.L. Carabb, K.H. Heffels, G. Seibert, in *Proceedings of the International Colloquium ECOSEC*, Toulouse, 1970 (Gordon and Breach, New York, 1971), p. 349
8. H. Fang, X. Li, S. Song, Y. Xu, J. Zhu, Nanotechnology **19**, 255703 (2008)
9. E.C. Garnett, P. Yang, J. Am. Chem. Soc. **130**, 9224 (2008)
10. M.D. Kelzenberg, D.B. Turner-Evans, B.M. Kayes, M.A. Filier, M.C. Putnam, N.S. Lewis, H.A. Atwater, Nano. Lett. **8**, 710 (2008)
11. T. Stelzner, M. Pietsch, G. Andrä, F. Falk, E. Ose, S. Christiansen, Nanotechnology **19**, 295203 (2008)
12. L. Hu, G. Chen, Nano. Lett. **7**, 3249 (2007)
13. B.M. Kayes, H.A. Atwater, N.S. Lewis, J. Appl. Phys. **97**, 114302 (2005)
14. J. Zhu, Z. Yu, G.F. Burkhard, C.-M. Hsu, S.T. Connor, Y. Xu, Q. Wang, M. McGehee, S. Fan, Y. Cui, Nano. Lett. **9**, 279 (2008)
15. J. Li, H. Yu, S.M. Wong, G. Zhang, X. Sun, P.G.Q. Lo, D.L. Kwong, Appl. Phys. Lett. **95**, 033102 (2009)
16. Y.-F. Huang, S. Chattopadhyay, Y.-J. Jen, C.-Y. Peng, T.-A. Liu, Y.-K. Hsu, C.-L. Pan, H.-C. Lo, C.-H. Hsu, Y.-H. Chang, C.-S. Lee, K.-H. Chen, L.-C. Chen, Nat. Nanotech. **2**, 770 (2007)
17. R.A. Street, P. Qi, R. Lujan, W.S. Wong, Appl. Phys. Lett. **93**, 163109 (2008)
18. K.Q. Peng, Y.J. Yan, S.P. Gao, J. Zhu, Adv. Mater. **14**, 1164 (2002)
19. K. Peng, Z. Huang, J. Zhu, Adv. Mater. **16**, 73 (2004)
20. K. Peng, Y. Xu, Y. Wu, Y. Yan, S.T. Lee, J. Zhu, Small **1**, 1062 (2005)
21. M.L. Zhang, K.Q. Peng, X. Fan, J.S. Jie, R.Q. Zhang, S.T. Lee, N.B. Wong, J. Phys. Chem. C **112**, 4444 (2008)
22. Z. Huang, H. Fang, J. Zhu, Adv. Mater. **19**, 744 (2007)
23. F. Burmeister, C. Schäfle, T. Matthes, M. Böhmisch, J. Boneberg, P. Leiderer, Langmuir **13**, 2983 (1997)
24. C. Levy-Clement, A. Lagoubl, M. Neumann-Spallart, M. Rodot, R. Tenne, J. Electrochem. Soc. **138**, L69 (1991)
25. V. Yerokhov, I. Melnyk, A. Tsisaruk, I. Semochko, Opto-Electron. Rev. **4**, 414 (2000)
26. B.S. Kim, D.H. Lee, S.H. Kim, G.H. An, K.J. Lee, N.V. Myung, Y.H. Choa, J. Am. Ceram. Soc. **92**, 2415 (2009)
27. K. Sahoo, M.-K. Lin, E.-Y. Chang, Y.-Y. Lu, C.-C. Chen, J.-H. Huang, C.-W. Chang, Nanoscale Res. Lett. **4**, 680 (2009)
28. L. Tsakalakos, J. Balch, J. Fronheiser, M.-Y. Shih, S.F. LeBoeuf, M. Pietrzykowski, P.J. Codella, B.A. Korevaar, J. Nanophoton **1**, 013552 (2007)
29. W.L. Min, B. Jiang, P. Jiang, Adv. Mater. **20**, 3914 (2008)
30. M.A. Green, *Solar Cells: Operating Principles, Technology and System Applications* (Prentice-Hall, Inc, Englewood Cliffs, NJ, 1982), p. 274
31. E.E. van Dyk, E.L. Meyer, Renew. Energy **29**, 333 (2004)